Instability and reorientation of block copolymer microstructure by imposed electric fields

Saulo Orizaga and Karl Glasner
Department of Mathematics, University of Arizona, 617 N. Santa Rita Tucson, Arizona 85721, USA
(Received 2 March 2016; revised manuscript received 29 April 2016; published 16 May 2016)

The influence of electric fields on lamellar block copolymer microstructure is studied in the context of a density functional model and its sharp interface limit. A free boundary problem for domain interfaces of strongly segregated polymers is derived, which includes coupling of interface and electric field orientation. The linearized dynamics of lamellar configurations is computed in this context, leading to quantitative criteria for instability as a function of pattern wavelength, field magnitude, and orientation. Numerical simulations of the full model in two and three dimensions are used to study the nonlinear development of instabilities. In three dimensions, sufficiently large electric field magnitude always leads to instability. In two dimensions, the field has either stabilizing or destabilizing effects depending on the misorientation of the field and pattern. Even when linear instabilities are present, the dynamics can lead to stable corrugated domain interfaces which do not align with the electric field. Sufficiently high field strengths, on the other hand, produce topological rearrangement which may lead to alignment.

DOI: 10.1103/PhysRevE.93.052504

I. INTRODUCTION

The self-assembly properties of block copolymer (BCP) materials make them appealing for scientific inquiry and technological application [1–3]. There are a variety of strategies to direct the self-assembly of block copolymer microstructures [4–6] in order to obtain desired morphology and orientation. One way of accomplishing this is through external intervention such as shear flow or electromagnetic fields [6].

The contrasting dielectric properties of polymer species presents an opportunity to modulate the compositional energy by applying external electric fields [7,8]. This has been useful in creating pattern alignment [9–13] as well as dynamic control of phase morphology [14–16]. While the fundamental physics of this process is well understood at this point [17,18], related dynamic phenomena such as stability and topological rearrangement still pose unanswered questions.

In general, lamellar microstructures tend to align with an applied electric field. This is explained theoretically by observing that electrostatic energy is minimized when composition fluctuations $u = \exp(i\mathbf{k}\cdot\mathbf{x})$ have wave vectors $\mathbf{k}$ normal to an applied field [7]. This argument does not preclude the possibility of metastable equilibria where energy is only locally minimized, however. To investigate this situation, a detailed study of instabilities of predefined phases and subsequent morphological development is needed.

Onuki and Fukuda [19] were the first to theoretically compute the stability of a lamellar microstructure due to an external electric field. By expansion of a phenomenological free energy relevant for weak segregation, they find stability criteria for long-wavelength undulations. A more detailed calculation was made by Matsen [20,21], who used self-consistent field theory (SCFT) coupled to exact electrostatics to numerically evaluate stability of certain lamellar configurations.

The present work is motivated from the viewpoint of density functional models [22]. These have often proven to be more tractable than SCFT for simulations [23] and analytic studies [24,25], in particular to study strongly segregated polymer systems. In addition, this modeling paradigm has been used successfully to study pattern alignment and rearrangement of block copolymer morphologies due to electric fields [26–30]. In addition, this modeling paradigm allows an explicit description of interphase boundaries which arise in the limit of strong segregation.

Our work extends the stability analysis for lamellar morphologies in several ways. We determine a free boundary problem for the motion of interfaces which arise when microphase segregation is strong enough to form distinct monomer-rich domains. This description includes effects of field misalignment which potentially destabilizes interfaces. Analytic calculations for stability of layered interfaces can be carried explicitly in this limit (see, e.g., Refs. [25,31] for related work). We find that instability is determined not only by field strength and lamellar wavelength but also by the relative orientation of the field and interfaces. We also find that instability may be insufficient to initiate topological changes needed for complete pattern realignment.

This paper is organized as follows. In Sec. II we review the derivation of density functional models which include electrostatic energy coupled to monomer composition. In Sec. III, the sharp interface description of the density functional model is computed. This allows for explicit calculations of linearized stability of lamellar microstructures which is detailed in Sec. IV. The nonlinear development of instabilities and pattern alignment is studied numerically in Sec. V.

II. MODEL FORMULATION

Here we provide a brief recapitulation of the derivation and simplification of the free energy. We suppose that our system occupies a two- or three-dimensional domain Ω, with A-monomer density ψ and electric field ∇V, where V is the electrostatic potential. The free energy functional has the form [19,20,22]

$$F = \int_\Omega \frac{a}{2}|\nabla\psi|^2 + bg(\psi)d\mathbf{x} + \frac{c}{2}\int_\Omega\int_\Omega G(\mathbf{x}-\mathbf{y}) \times [\psi(\mathbf{x})-f][\psi(\mathbf{y})-f]\,d\mathbf{x}\,d\mathbf{y} - \frac{1}{2}\int_\Omega \varepsilon(\psi)|\nabla V|^2 d\mathbf{x},$$

where the electrostatic potential satisfies

$$\nabla\cdot[\varepsilon(\psi)\nabla V] = 0.$$

The coefficients a,b,c can be related to physical parameters involving molecular interactions and polymer characteristics [see, e.g., Ref. [22] and Eq. (4.19) in Ref. [32]]. The bulk energy potential $g(\psi)$ has minima which prefer homogeneous phases $\psi = 0$ and $\psi = 1$. A convenient choice used here is

$$g(\psi) = 32\psi^2(1-\psi)^2,$$

although other choices would lead to the same sharp interface description studied below. The long-range interaction kernel G is the Laplacian Green's function and f is the average volume fraction of A-monomer. The electric permittivity $\varepsilon(\psi)$ depends on local composition, which means that externally imposed fields can alter the energy landscape and resulting microsegregation patterns. In principle, high field strengths may lead to dielectric breakdown, but this is not considered here since the threshold for microstructure realignment is often much smaller than that for breakdown [8].

It is typical to simplify the electric field contribution by supposing that the permittivity depends only weakly on composition (e.g., Refs. [27,33]). While computations with exact electrostatics is feasible, our analytic theoretical results simplify considerably in this regime. Suppose that in absence of any compositional inhomogeneity there is an imposed field of magnitude E and direction $\mathbf{a}$. The potential can be written $V = E\mathbf{a}\cdot\mathbf{x} + V_p$ where V_p is periodic in space. It can be shown (see Appendix A) that at leading order,

$$\Delta V_p = -\frac{\varepsilon'(0)E}{\varepsilon(0)}\nabla\psi\cdot\mathbf{a}, \tag{1}$$

and the relevant electric field contribution to the free energy is

$$\frac{\varepsilon(0)}{2}\int_\Omega |\nabla V_p|^2\, d\mathbf{x}. \tag{2}$$

It should be noted that this result is still valid even when compositional changes become abrupt in the case of strong segregation (see Appendix A).

The free energy can be put into a form suitable for analysis by defining $u = 2\psi - 1$ and $\overline{u} = 2f - 1$ as the the compositional order parameter and its spatial average, respectively, and rescaling the free energy by dividing by $(ab)^{1/2}$ which gives (up to a multiplicative constant)

$$F = \int_\Omega \frac{\epsilon}{2}|\nabla u|^2 + \epsilon^{-1}W(u) + \frac{\alpha}{2}\int_\Omega\int_\Omega G(\mathbf{x}-\mathbf{y})[u(\mathbf{x})-\overline{u}] \times [u(\mathbf{y})-\overline{u})]\, d\mathbf{x}\, d\mathbf{y} + \frac{\beta}{2}\int_\Omega |\nabla\Phi|^2\, d\mathbf{x}, \tag{3}$$

where

$$\epsilon = \frac{a^{1/2}}{4b^{1/2}}, \quad \alpha = \frac{c}{4(ab)^{1/2}},$$

$$\beta = \frac{\varepsilon'(0)^2E^2}{4\varepsilon(0)(ab)^{1/2}}, \quad W(u) = \frac{1}{2}(u^2-1)^2,$$

and where the rescaled potential Φ satisfies

$$\Delta\Phi = -\nabla u\cdot\mathbf{a}. \tag{4}$$

Dynamics arise from diffusive kinetics so that, with an appropriate choice of time scale, $u_t = \Delta\mu$, where $\mu = \delta F/\delta u$ is the total chemical potential. The result is an extended version of the Ohta-Kawasaki equation

$$\epsilon u_t = \Delta v + \epsilon\alpha(\overline{u}-u) + \epsilon\beta(\nabla^2 u\cdot\mathbf{a})\cdot\mathbf{a}, \tag{5}$$

$$v = -\epsilon^2\Delta u - 2u(1-u^2). \tag{6}$$

The quantity v has the physical meaning of a partial chemical potential associated with phase-separating compositional free energy.

Our interest is in a case where predominantly lamellar microstructures have characteristic wavelength much smaller than the physical domain size. To this end, we will consider Eq. (5) on rectangular domains in dimensions two and three, subject to periodic boundary conditions.

III. SHARP INTERFACE LIMIT

The limit of small ϵ is now considered, representing a regime of strong polymer segregation. The method of matched asymptotic expansions is used to derive a free boundary problem satisfied by phase interfaces. The calculation is an extension of that done for the classical Cahn-Hilliard equation [34] and for the Ohta-Kawasaki equation [24]. The applicability of the free boundary problem to the case of intermediate segregation strength is investigated numerically later on in Sec. V C.

A. Asymptotic expansions

It is supposed that the monomer-rich subdomains $\Omega_\pm = \{\pm u > 0\}$ are separated by an interface $\Gamma = \{u = 0\}$. Expansions in ϵ are performed both away from the interface and near the interface using a stretched, moving, local fitted coordinate system. Here we summarize the results of this calculation. More details are found in Appendix B.

Away from the interface Γ we expand $u = u_0 + \epsilon u_1 + \epsilon^2 u_2 + \cdots$ and $v = v_0 + \epsilon v_1 + \epsilon^2 v_2 + \cdots$. At leading order this gives $u_0 = \pm 1$ and $v_0 = 0$ for subdomains $\Omega_\pm$. The correction terms satisfy $u_1 = \frac{1}{4}v_1$ with v_1 solving

$$\Delta v_1 = -\alpha(\bar{u} - u_0), \tag{7}$$

which is supplemented by interface conditions on Γ which derive from asymptotic matching.

The inner expansion is done in a standard orthogonal coordinate system (ρ,s_1,s_2) fitted to Γ. The coordinate $\rho = \epsilon^{-1}r$ is chosen so that r is the signed distance to Γ (with $r > 0$ in Ω_+), and $s_{1,2}$ are chosen so they measure arc length in their corresponding directions along Γ. As a conventional choice, the normal vector $\mathbf{n}$ to Γ will always be in the direction toward the subdomain Ω_+. The coordinates are aligned with the Darboux frame on Γ so that varying s_j produce curves with tangent vectors $\mathbf{t}_j$ which are aligned with the principal directions at each point on the interface. Corresponding to the principle directions are (normal) curvatures κ_1 and κ_2 so that $\kappa = \kappa_1 + \kappa_2$ is the mean curvature of Γ. As a conventional choice, these will be oriented so that $\kappa > 0$ when the subdomain Ω_- is locally convex.

The inner expansion takes the form $u = U(\rho,s_1,s_2,t) = U_0 + \epsilon U_1 + \epsilon^2 U_2 + \cdots$ and $v = V(\rho,s_1,s_2,t) = V_0 + \epsilon V_1 + \epsilon^2 V_2 + \cdots$. To leading order one finds the typical interface profile $U_0 = \tanh(\rho)$. The next order gives $V_1 = \beta(\mathbf{n}\cdot\mathbf{a})^2(-U_0 \pm 1) + v_1(0\pm,s_1,s_2,t)$, where $\pm$ refers to limits from either side of the interface. A solvability argument then yields boundary conditions for (7) on each side of the interface

$$v_1(0\pm,s,t) + \beta(\mathbf{n}\cdot\mathbf{a})^2(\pm 1) = -\tfrac{2}{3}\kappa.$$

The next order gives a dynamic equation

$$\begin{aligned} r_t U_{0\rho} =& V_{2\rho\rho} - \beta(\mathbf{n}\cdot\mathbf{a})^2 U_{0\rho} + U_{1\rho\rho}(\mathbf{n}\cdot\mathbf{a})^2 \\ &+ \kappa U_{0\rho}[\kappa_1(\mathbf{t}_1\cdot\mathbf{a})^2 + \kappa_2(\mathbf{t}_2\cdot\mathbf{a})^2], \end{aligned} \tag{8}$$

which, by asymptotic matching, relates the interface velocity to the difference in chemical potential gradients

$$\begin{aligned} r_t =& \tfrac{1}{2}[v_{1r}(0+,\cdot) - v_{1r}(0-,\cdot)] - \beta\kappa(\mathbf{n}\cdot\mathbf{a})^2 \\ &+ \beta[\kappa_1(\mathbf{t}_1\cdot\mathbf{a})^2 + \kappa_2(\mathbf{t}_2\cdot\mathbf{a})^2]. \end{aligned} \tag{9}$$

B. Free boundary problem

With the identification of the leading order normal velocity V_n of the front with $-r_t$, the above results can be summarized as a free boundary evolution:

$$\Delta v = -\alpha(\overline{u} \mp 1) \quad \text{on } \Omega_\pm, \tag{10}$$

$$v \pm \beta(\mathbf{n}\cdot\mathbf{a})^2 = -\tfrac{2}{3}\kappa, \quad \text{on } \partial\Omega_\pm, \tag{11}$$

$$\begin{aligned} V_n =& -\tfrac{1}{2}[\partial v/\partial n]_-^+ + \beta\kappa(\mathbf{n}\cdot\mathbf{a})^2 \\ &- \beta[\kappa_1(\mathbf{t}_1\cdot\mathbf{a})^2 + \kappa_2(\mathbf{t}_2\cdot\mathbf{a})^2], \end{aligned} \tag{12}$$

where $[]_-^+$ refers to the jump across the interface, and $\partial\Omega_\pm$ refers to taking a one-sided limit from either the Ω_+ or Ω_- subdomain. In two dimensions, one can use $(\mathbf{t}_1\cdot\mathbf{a})^2 = 1 - (\mathbf{n}\cdot\mathbf{a})^2$ and $\kappa = \kappa_1$ so that (12) simplifies to

$$V_n = -\tfrac{1}{2}[\partial v/\partial n]_-^+ + \beta\kappa\left[2(\mathbf{n}\cdot\mathbf{a})^2 - 1\right]. \tag{13}$$

C. Energy dissipation in the free boundary problem

The sharp interface problem has the corresponding free energy

$$E = \frac{4}{3}\int_\Gamma dA + \int_\Omega \frac{\alpha}{2}|\nabla w|^2 + \frac{\beta}{2}|\nabla\Phi|^2\, d\mathbf{x}, \tag{14}$$

where the potentials w, Φ solve (subject to periodic boundary conditions)

$$\Delta w = \overline{u} \mp 1 \quad \text{on } \Omega_\pm \tag{15}$$

and

$$\Delta\Phi = 2\delta_\Gamma(\mathbf{n}\cdot\mathbf{a}), \tag{16}$$

where δ_Γ is a delta function measure concentrated along the interface. The terms in (14) refer to the surface energy, the energy of polymer stretching, and the electrostatic energy, respectively. We note that this is similar to the decomposition of energy into interfacial and stretching components as in SCFT strong stretching theory [35,36]. In this respect, the sharp interface description of interphase boundaries does not have to rely on a connection to the underlying phase field model but could be regarded as a strong stretching theory in its own right.

It can be shown that the rate of energy dissipation is

$$\frac{dE}{dt} = \int_{\partial\Omega_+} \mu\frac{\partial\mu}{\partial n}\, d\mathbf{x} - \int_{\partial\Omega_-} \mu\frac{\partial\mu}{\partial n}\, d\mathbf{x} = -\int_\Omega |\nabla\mu|^2\, d\mathbf{x}, \tag{17}$$

which is the usual expression (up to a kinetic constant) for systems driven by mass flux arising from gradients of the sharp interface chemical potential

$$\mu = v + \alpha w + \mu_e, \quad \mu_e \equiv \beta\nabla\Phi\cdot\mathbf{a}.$$

Details of the derivation are given in Appendix C.

D. Dimensionless formulation of the free boundary problem

The parameter α sets an equilibrium length scale L_{eq} via $L_{\text{eq}} = \alpha^{-1/3}$. It is understood that for the lamellar BCP phase, this length is proportional to the stripe width which minimizes the free energy ([32]). The parameter α can be eliminated by scaling lengths by L_{eq}:

$$\begin{aligned} &x' = x/L_{\text{eq}}, \quad v' = L_{\text{eq}}v, \quad \kappa' = L_{\text{eq}}\kappa, \\ &\beta' = L_{\text{eq}}\beta, \quad t' = t/L_{\text{eq}}^3. \end{aligned}$$

The free boundary problem (10)–(12) becomes (after dropping primes)

$$\Delta v = -(\overline{u} \mp 1) \quad \text{on } \Omega_\pm, \tag{18}$$

$$v \pm \beta(\mathbf{n}\cdot\mathbf{a})^2 = -\tfrac{2}{3}\kappa, \quad \text{on } \partial\Omega_\pm, \tag{19}$$

$$V_n = -\tfrac{1}{2}[\partial v/\partial n]_-^+ + \beta\kappa(\mathbf{n}\cdot\mathbf{a})^2 - \beta[\kappa_1(\mathbf{t}_1\cdot\mathbf{a})^2 + \kappa_2(\mathbf{t}_2\cdot\mathbf{a})^2]. \tag{20}$$

IV. STABILITY OF LAMELLAR MICROSTRUCTURE

The reduced model (18) – (20) provides an opportunity to analytically study stability of lamellar microstructures. This is done by linearization about a preexisting phase and computing the growth rates associated with interface perturbations (e.g., Refs. [25,31]). Instabilities may lead to topological rearrangement of microphase domains and possible alignment of electric field and interface orientation. The latter depends on the full nonlinear evolution and is studied numerically in Sec. V.

A. Growth rates of perturbed interfaces

We now consider the stability of a a defect-free lamellar pattern whose interface normals are oriented in the z direction. These interfaces are described by graphs $z = z_{0j}(x,y) = j\ell$ for j even and $z = z_{0j}(x,y) = \ell(1+\overline{u}) + j\ell$ for j odd. Here 2ℓ is the wavelength associated with the periodic lamellar structure and is assumed to be much smaller than the physical domain size so that confinement effects can be ignored. The corresponding solution to (10) is $v = v_0(z)$ where

$$\begin{aligned} v_0(z) =& -\frac{(\overline{u}-1)}{2}z[z - \ell(1+\overline{u})] - \beta(\mathbf{n}_0\cdot\mathbf{a})^2, \\ & 0 < z < \ell(1+\overline{u}), \end{aligned} \tag{21}$$

$$v_0(z) = \frac{(\overline{u}+1)}{2}[\ell(1+\overline{u}) - z](z-2\ell) + \beta(\mathbf{n}_0\cdot\mathbf{a})^2,$$
$$\ell(1+\overline{u}) < z < 2\ell. \tag{22}$$

We will consider instabilities of two types: "wriggled," where perturbations take the form

$$z_j(x,y) = z_{0j} + \delta\exp(i\mathbf{k}\cdot\mathbf{x}+\sigma t) + \text{c.c.}, \tag{23}$$

and "varicose" perturbations

$$z_j(x,y) = z_{0j} + (-1)^j\delta\exp(i\mathbf{k}\cdot\mathbf{x}+\sigma t) + \text{c.c.} \tag{24}$$

Here $\mathbf{k}\in\mathbb{R}^2$ is the transverse wave vector, $\mathbf{x}=(x,y)$ and c.c. refers to complex conjugates of the preceding terms so that z_j are real valued. The two-dimensional case is handled in parallel by suppressing the second component of $\mathbf{k}$. The perturbation is assumed small, i.e., $|\delta|\ll 1$, so that one can expand

$$v = v_0 + \delta v_1 + \text{c.c.} + O(\delta^2).$$

For convenience, we work with a complex-valued field v_1, which solves $\Delta v_1 = 0$ with boundary conditions for the wriggled case

$$v_1[x,y,\ell(1+\overline{u})] = \exp(i\mathbf{k}\cdot\mathbf{x}+\sigma t)\left\{\frac{2k^2}{3} - v_{0z}[x,y,\ell(1+\overline{u})] - \beta\tilde{n}\right\}, \tag{25}$$

$$v_1(x,y,0) = \exp(i\mathbf{k}\cdot\mathbf{x}+\sigma t)\left[-\frac{2k^2}{3} - v_{0z}(x,y,0) - \beta\tilde{n}\right], \tag{26}$$

for the domain $0<y<\ell(1+\overline{u})$ and

$$v_1(x,y,2\ell) = \exp(i\mathbf{k}\cdot\mathbf{x}+\sigma t)\left[-\frac{2k^2}{3} - v_{0z}(x,y,2\ell) - \beta\tilde{n}\right], \tag{27}$$

$$v_1[x,y,\ell(1+\overline{u})] = \exp(i\mathbf{k}\cdot\mathbf{x}+\sigma t)\left\{\frac{2k^2}{3} - v_{0z}[x,y,\ell(1+\overline{u})] - \beta\tilde{n}\right\}, \tag{28}$$

for $\ell(1+\overline{u})<z<2\ell$. The term $\tilde{n} = -2(\mathbf{n}_0\cdot\mathbf{a})(\mathbf{n}_1\cdot\mathbf{a})$ where $\mathbf{n}_0 = (-1)^j(0,0,1)$ and $\mathbf{n}_1 = (-1)^j e^{i\mathbf{k}\cdot\mathbf{x}}(\mathbf{k},0)$ for the jth interface. The varicose case gives a similar problem, with signs reversed on the right-hand sides of (25) and (28). The solution for v_1 has the form

$$v_1 = e^{i\mathbf{k}\cdot\mathbf{x}+\sigma t}\begin{cases}\psi_1 e^{-kz} + \psi_2 e^{kz} & 0<z<\ell(1+\overline{u}),\\ \eta_1 e^{-kz} + \eta_2 e^{kz} & \ell(1+\overline{u})<z<2\ell,\end{cases} \tag{29}$$

where $k=|\mathbf{k}|$. Inserting into (25)–(28) gives a linear system for coefficients, which are found to be

$$\psi_1 = -\frac{-\frac{2k^2}{3} - \frac{1}{2}\ell(\overline{u}^2-1) + \tilde{n}\beta - e^{k\ell(1+\overline{u})}\left[\frac{2k^2}{3} + \frac{1}{2}\ell(\overline{u}^2-1) + \tilde{n}\beta\right]}{e^{-k\ell(1+\overline{u})} - e^{k\ell(1+\overline{u})}},$$

$$\psi_2 = \frac{4k^2 + 3\ell(\overline{u}^2-1)}{6(-1+e^{k\ell(1+\overline{u})})} - \frac{\tilde{n}\beta}{1+e^{k\ell(1+\overline{u})}},$$

$$\eta_1 = \frac{e^{\frac{3}{2}k\ell(3+\overline{u})}\left\{[4k^2+3\ell(\overline{u}^2-1)]\cosh\left[\frac{1}{2}k\ell(-1+\overline{u})\right] + 6\tilde{n}\beta\sinh\left[\frac{1}{2}k\ell(-1+\overline{u})\right]\right\}}{3(e^{4k\ell} - e^{2k\ell(1+\overline{u})})},$$

$$\eta_2 = -\frac{e^{k\ell}\{e^{k\ell\overline{u}}[4k^2+3\ell(\overline{u}^2-1) - 6\tilde{n}\beta] + e^{k\ell}[4k^2+3\ell(\overline{u}^2-1) + 6\tilde{n}\beta]\}}{6(e^{4k\ell} - e^{2k\ell(1+\overline{u})})}.$$

The linearized interface velocity (20) for $j=0$ is

$$V_n = \sigma(\mathbf{k})e^{i\mathbf{k}\cdot\mathbf{x}+\sigma t},$$

where the growth rate is

$$\sigma(\mathbf{k}) = e^{i\mathbf{k}\cdot\mathbf{x}+\sigma t}\left\{\frac{k}{2}(\psi_1 - \psi_2 - \eta_1 + \eta_2) + \beta\kappa\left[(\mathbf{n}_0\cdot\mathbf{a})^2 - \frac{(\mathbf{k}'\cdot\mathbf{a})^2}{k^2}\right]\right\} \tag{30}$$

with $\mathbf{k}' = (\mathbf{k},0)$. The last term derives from the fact that the principle directions on the (plane wave-shaped) perturbed surface are $\mathbf{t}_1 = (-k_y,k_x,0)/k$ and $\mathbf{t}_2 = (k_x,k_y,0)/k$ with curvatures 0 and k^2, respectively.

Since our interest is in the fastest growing mode, for the three-dimensional case this occurs when $\mathbf{k}'\cdot\mathbf{a}=0$. Therefore the last term in (30) can be suppressed, and the associated real part of the growth rate is

$$\sigma_{\text{wr}}(k) = \frac{e^{k\ell\overline{u}}(-1+e^{2k\ell})k[4k^2+3\ell(-1+\overline{u}^2])}{6(-e^{k\ell}+e^{k\ell\overline{u}})(-1+e^{k\ell(1+\overline{u})})} - 1 + \overline{\beta}k^2, \tag{31}$$

whereas for the varicose situation it is

$$\sigma_{\rm var}(k) = -\frac{e^{k\ell\overline{u}}(-1+e^{2k\ell})k[4k^2+3\ell(-1+\overline{u}^2)]}{6(e^{k\ell}+e^{k\ell\overline{u}})(1+e^{k\ell(1+\overline{u})})} - 1+\overline{\beta}k^2. \quad (32)$$

Here the combined effect of the electric field magnitude and direction is encoded in the parameter $\overline{\beta}$ where

$$\overline{\beta} = \overline{\beta}_{3d} = \beta(\mathbf{n}_0\cdot\mathbf{a})^2. \quad (33)$$

This means that in three dimensions, an imposed field always leads to a greater growth rate, unless the normal to the interface and electric field are exactly perpendicular.

In two dimensions, there is no freedom to choose the direction of $\mathbf{k}$. This means that the last term in (30) cannot be ignored. The consequence is that the effective electric field parameter is now

$$\overline{\beta} = \overline{\beta}_{2d} = \beta[2(\mathbf{n}_0\cdot\mathbf{a})^2 - 1] = \beta(2\sin^2\theta - 1),$$

where θ is the angle between the stripe orientation (the interface tangent plane) and electric field direction. It follows that if the field and lamellar orientation are misaligned by more that 45 degrees, the imposed field has a potentially destabilizing effect, whereas if it is less it has a *stabilizing* property.

B. Stability in the absence of electric fields

We first consider the situation where no external field is present. For the particular case of even mixtures $\overline{u}=0$ and $\overline{\beta}=0$, the real part of the growth rates (31) and (32) becomes

$$\sigma_{\rm wr}(k) = -1+\frac{1}{6}k(-4k^2+3\ell)\coth\left[\frac{k\ell}{2}\right],$$
$$\sigma_{\rm var}(k) = -1+\frac{1}{6}k(-4k^2+3\ell\alpha)\tanh\left[\frac{k\ell}{2}\right]. \quad (34)$$

In this case it is easy to see that the wriggled instability predominates over the varicose.

For arbitrary $\overline{u}$, it is possible to analytically identify the threshold for the wriggled instability. Since $\sigma_{\rm wr}(k)\to 0$ as $k\to 0$, the expression (31) can be approximated for small k. Long wavelength instability occurs when

$$\ell^3 > \frac{16}{(\overline{u}^2-1)^2}. \quad (35)$$

This is consistent with the quantitative results in Ref. [31], where it is noted that the energy minimizing period of a lamellar state is proportional to the pattern wavelength at the onset of instability.

For the varicose case, instability first occurs at a finite wavelength, and the fastest growing mode must be determined numerically. The computed neutral stability curves for both the varicose and wriggled cases are are shown in Fig. 1. The axes are in terms of physical quantities, the monomer volume fraction $f=(\overline{u}+1)/2$, and the ratio of imposed lamellar spacing to equilibrium pattern length $\ell = L/L_{\rm eq}$.

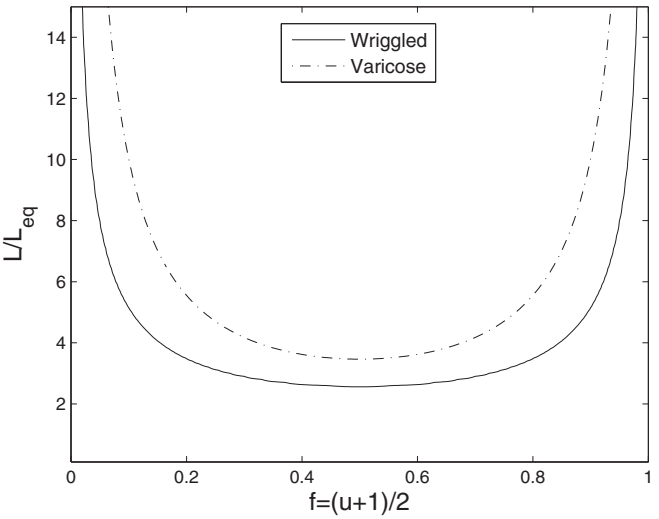

FIG. 1. Neutral stability curves for wriggled and varicose perturbations in the absence of electric field ($\overline{\beta}=0$). The unstable region lies above the curves.

C. Effect of electric field

We now consider the stability of a lamellar structure for various field intensities. The neutral stability curves for different values of $\overline{\beta}$ are shown in Figs. 2 and 3. The instability is suppressed for $\overline{\beta}<0$, which can happen only in the two-dimensional case when the misorientation angle is less than $\pi/4$. In contrast, instability becomes more likely as $\overline{\beta}$ increases.

For the varicose mode, we find that for sufficient field intensity ($\overline{\beta}\approx> 1$), instability is always present for all but extremely asymmetric volume fraction mixtures.

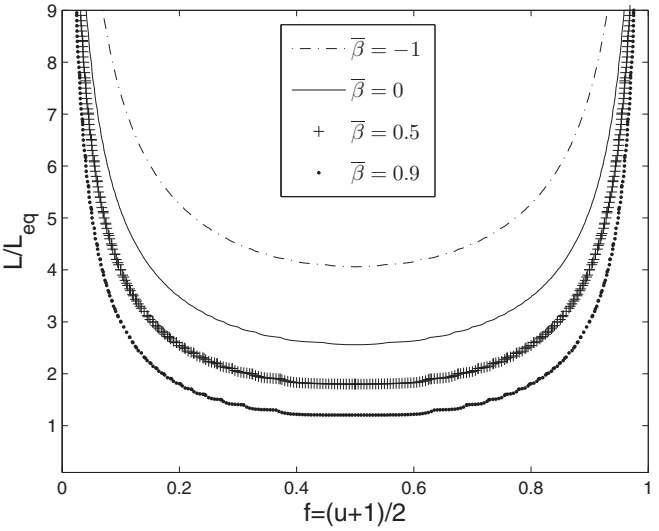

FIG. 2. Neutral stability curve for wriggled modes. As the electric field parameter $\overline{\beta}$ increases, instability becomes more likely. Negative values $\overline{\beta}<0$ (possible only in two dimensions) have a stabilizing effect. The unstable region lies above the curves.

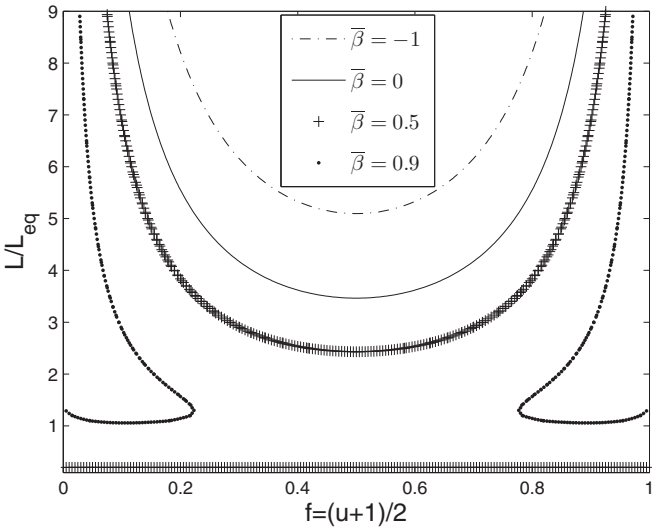

FIG. 3. Neutral stability curve for varicose modes. As the electric field parameter $\overline{\beta}$ increases, instability becomes more likely. The unstable region lies above the curves for $\overline{\beta} \leqslant 0.5$, whereas for large $\overline{\beta}$ is large enough, this region extends to small L/L_{eq} as well.

V. NONLINEAR EVOLUTION OF UNSTABLE INTERFACES

Electric fields of sufficient intensity and misorientation may destabilize lamellar interfaces. On the other hand, the evolution of the instability may or may not result in a complete realignment of the microstructure. We find that the bifurcation of steady solutions as $\overline{\beta}$ is increased can be supercritical, so that the growth of the instability saturates. This may lead to a corrugated lamellar microstructure whose alignment is not significantly altered. In this case, large-scale changes in morphology only occur at sufficient field strength far beyond the point of linear instability.

To investigate the nonlinear development of the instabilities which were discovered in Sec. IV, we implement numerical simulations in two and three dimensions. These are based on variational, semi-implicit, pseudo-spectral methods described elsewhere [37], which are suitable for energy-driven pattern formation equations like (5). Simulations are conducted on a square or cubic domain endowed with periodic boundary conditions to mimic a small portion of a larger material sample.

A. Two dimensions

Two-dimensional simulations of (5) were conducted over a wide range of values of the field parameter β. The initial conditions were chosen to be a perfectly lamellar configuration oriented perpendicular to the field, in a domain of dimensionless size $2\pi \times 2\pi$. The parameters for interface thickness and stretching energy were $\epsilon = 0.1$ and $\alpha = 1.0$, respectively.

A small amount of noise was added to the initial condition to initiate instability. Figure 4 shows the evolution (from left to right) at times $t = 0.15, 0.20, 0.25$, and 0.30, for various values for the electric field parameter $\overline{\beta} = 5, 6.5, 8$, and 9.5 (from top to bottom).

In the weak field regime just beyond the threshold for instability (first row, Fig. 4), the lamellar pattern evolves to a steady, corrugated pattern. Even when the varicose instabilities are visible (second row, Fig. 4), the domain orientation remains effectively the same as the initial condition. For larger field strengths (third and fourth rows, Fig. 4), varicose modes grow and cause pinching of striped domains, followed by topological transitions to a nearly amorphous state. Stripes then re-form, with orientation roughly the same as the electric field. We note that this process can select a different pattern wavelength than that originally imposed by the initial condition.

B. Three dimensions

Fully three dimensional simulations were also conducted to observe microstructure alignment from a disordered microstructure. The domain size was $(2\pi)^3$, and the simulation parameters were $\alpha = 15, \epsilon = 0.1$. The field was oriented along the y axis of the simulation box with strength $\beta = 10$. Equation (5) was first solved without the electric field using random initial data, until a discernible pattern without long-range order emerged (Fig. 5, left). The field was then turned on, and the pattern stretches in the y direction. Eventually this creates alignment in this direction, but the morphology remains labyrinthine in the transverse directions. A well-ordered lamellar structure does not emerge from this scenario since the field has no effect on interfaces which are aligned with it.

To produce alignment along two axes which leads to lamellar structures, we investigated alternating the direction of the field. Figure 6 shows the results of a simulation ($\overline{\beta} = 15, \alpha = 18, \epsilon = 0.1$) where an initially lamellar pattern was first subject to a field with the direction along the x axis, which produces stretching along this direction (Fig. 6 top right). Then the electric field orientation was alternated to be parallel to the y axis. The labyrinthine structure stretches along this direction, producing some dislocations (Fig. 6 lower left). Finally, alternating the electric field orientation back to the x-axis direction allows for the minor imperfections in the lamellar structure to be fully eliminated (Fig. 6 lower right).

Reorientation of the lamellar structure in three space dimensions can be observed even when the field is only slightly misaligned from the interfaces. To demonstrate this, we apply an electric field that is 20 degrees out of alignment from the orientation of the lamellar structure. The same parameters as in Fig. 6 were used. The nonlinear evolution is captured at various times in Fig. 7. Both wriggled and varicose instabilities are observed and grow to allow topological changes and reorientation. We note that stripes at the imposed angle are incommensurate with the size of the domain, and topological defects are necessarily created.

C. Effect of finite interface thickness

It is important to investigate the quantitative validity of our results in cases where the interface width is not particularly small, since many copolymer systems lie in a regime of intermediate segregation. Numerical simulations using the setup of Sec. V A were used to explore the dependence of the linear evolution of a perturbed striped state for different values of ϵ.

In Fig. 8 we compare the neutral stability curves for wriggled modes in the sharp interface limit (dotted) to the

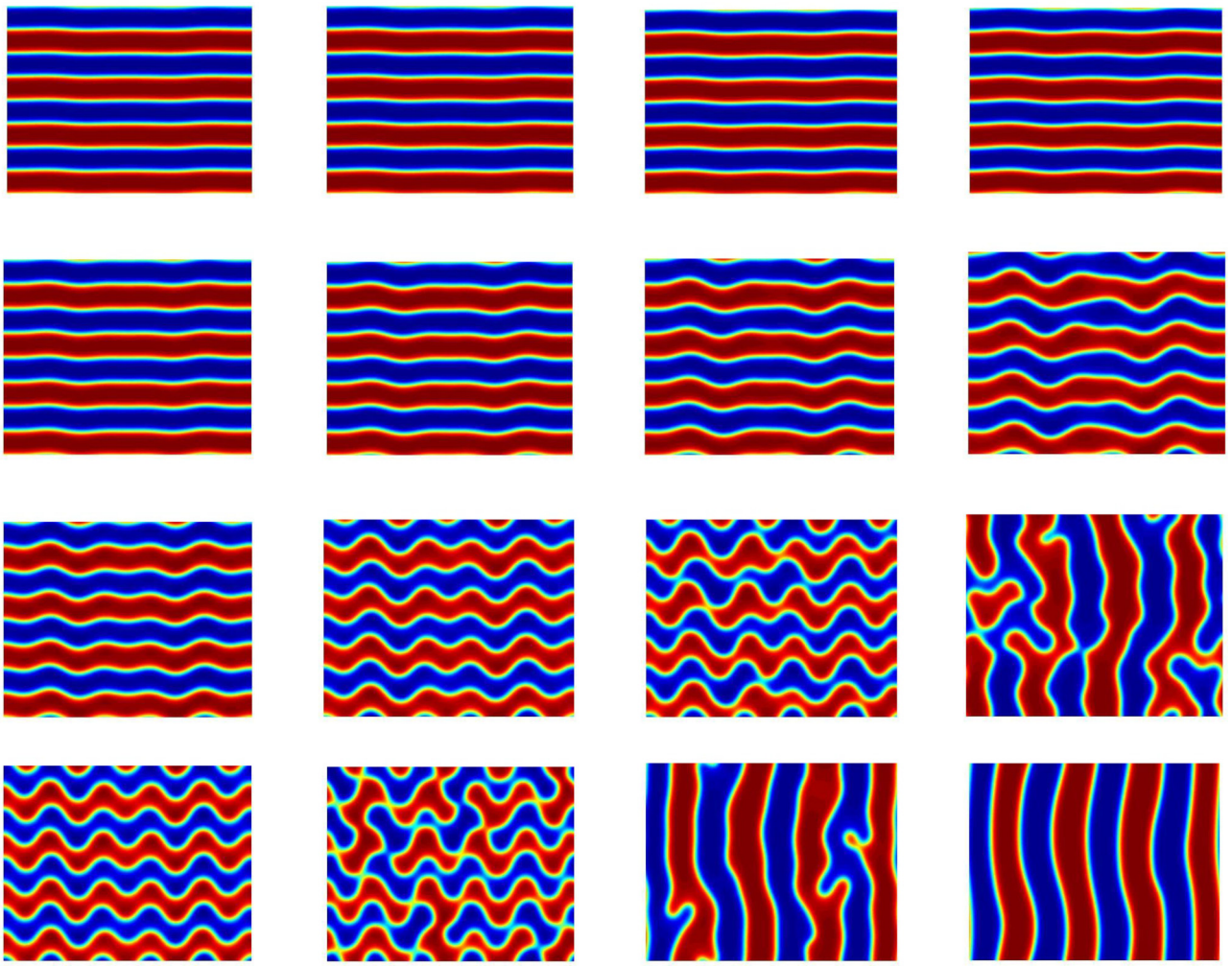

FIG. 4. Nonlinear evolution of the electric-field induced instability of a two-dimensional lamellar film. Lateral increments at $t = 0.15, 0.20, 0.25$, and 0.30 (from left to right) and vertical increments for the intensity of the electric field $\overline{\beta} = 5, 6.5, 8$, and 9.5 (top to bottom).

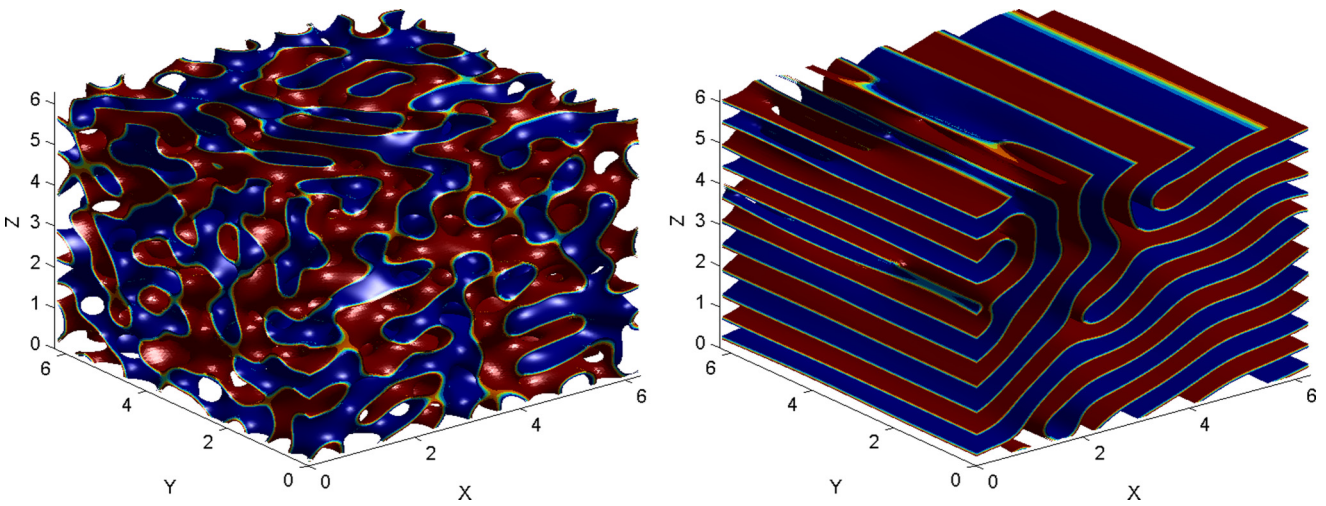

FIG. 5. Three-dimensional simulations of (5) subject to an electric field aligned along the y axis. Left: Snapshot at time $t = 400$ with $\overline{\beta} = 0$, $\alpha = 15$, and $\epsilon = 0.1$. Right: Snapshot taken at $t = 800$ and where field strength is $\overline{\beta} = 10$, showing reorientation of the microstructure in the direction of the field.

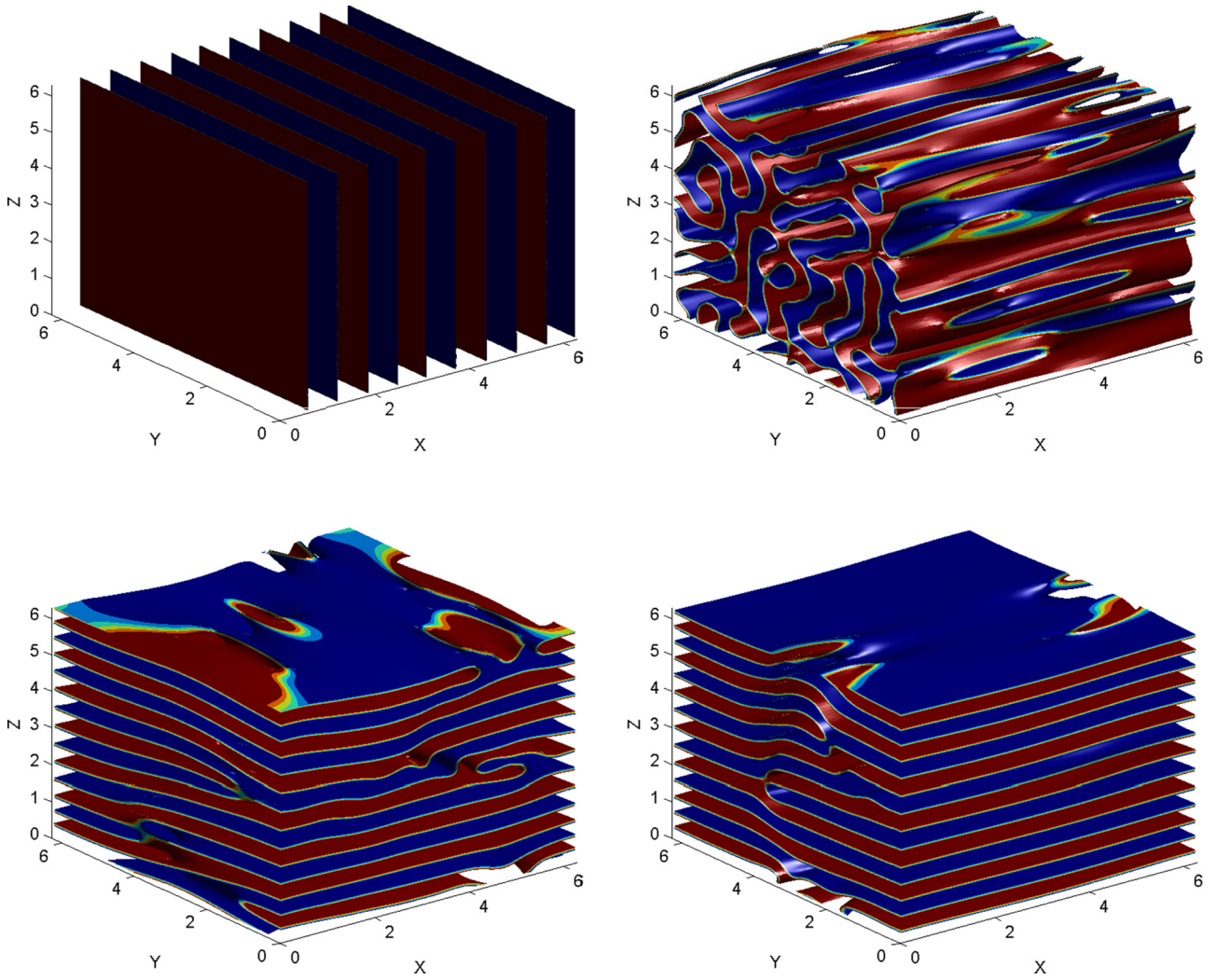

FIG. 6. Three-dimensional simulations of (5) subject to an electric field that alternates in the x and y direction. Top left: Initial lamellar state at time $t = 0$ with $\overline{\beta} = 15$, $\alpha = 18$, and $\epsilon = 0.1$. Top right: $t = 25$, where the electric field is oriented along the x axis. Bottom left: Time $t = 50$, where the electric field is oriented along the y axis. Bottom right: Time $t = 75$ where the electric field is again oriented along the x axis. Alternating the field direction produces a reoriented lamellar pattern.

numerically computed neutral stability curves as ϵ is varied. This was done both for the case of no electric field and also where $\beta = 1$ where the field is initially perpendicular to the stripes. In the case of no field, the threshold for instability varied only by $\approx 20\%$ even when the diffuse interface width was comparable to the stripe width. With the field turned on, the threshold varied by a factor of about 2 as ϵ was increased. This suggests that the linear stability predictions in the sharp interface problem are a reasonable guideline for the stability of lamellar structures even in the weak segregation regime. We note that smaller ϵ, i.e., greater segregation, has a systematically stabilizing effect with or without an imposed electric field.

VI. DISCUSSION AND CONCLUSIONS

This paper provides a quantitative explanation for the preference for lamellar microstructures to align with electric fields. Stability of interfaces was shown to be a function of both field orientation and intensity. The field can either be stabilizing or destabilizing in two dimensions, depending the amount of misalignment. In three dimensions, in contrast, any amount of field misalignment can produce instability, providing the field intensity is high enough. On the other hand, interface instabilities are not always sufficient to produce the morphological transitions which cause widespread realignment. This is observed to occur only for field strengths well beyond the linear instability threshold.

Our results indicate that for intermediate and strong segregation regimes, microstructure realignment occurs by topological rearrangements of interfaces. This should be contrasted to the results of Pinna *et al.* [38], who study the weakly segregated regime. They find two possible mechanisms for realignment: partial melting of the ordered phase and pattern rotation. The first cannot happen here, since it is relevant only near the order-disorder transition where interfaces are not well defined. We have not observed the second mechanism in our simulations either.

We find that in most cases, the wriggled modes are the ones which destabilize first. This is consistent with the theoretical

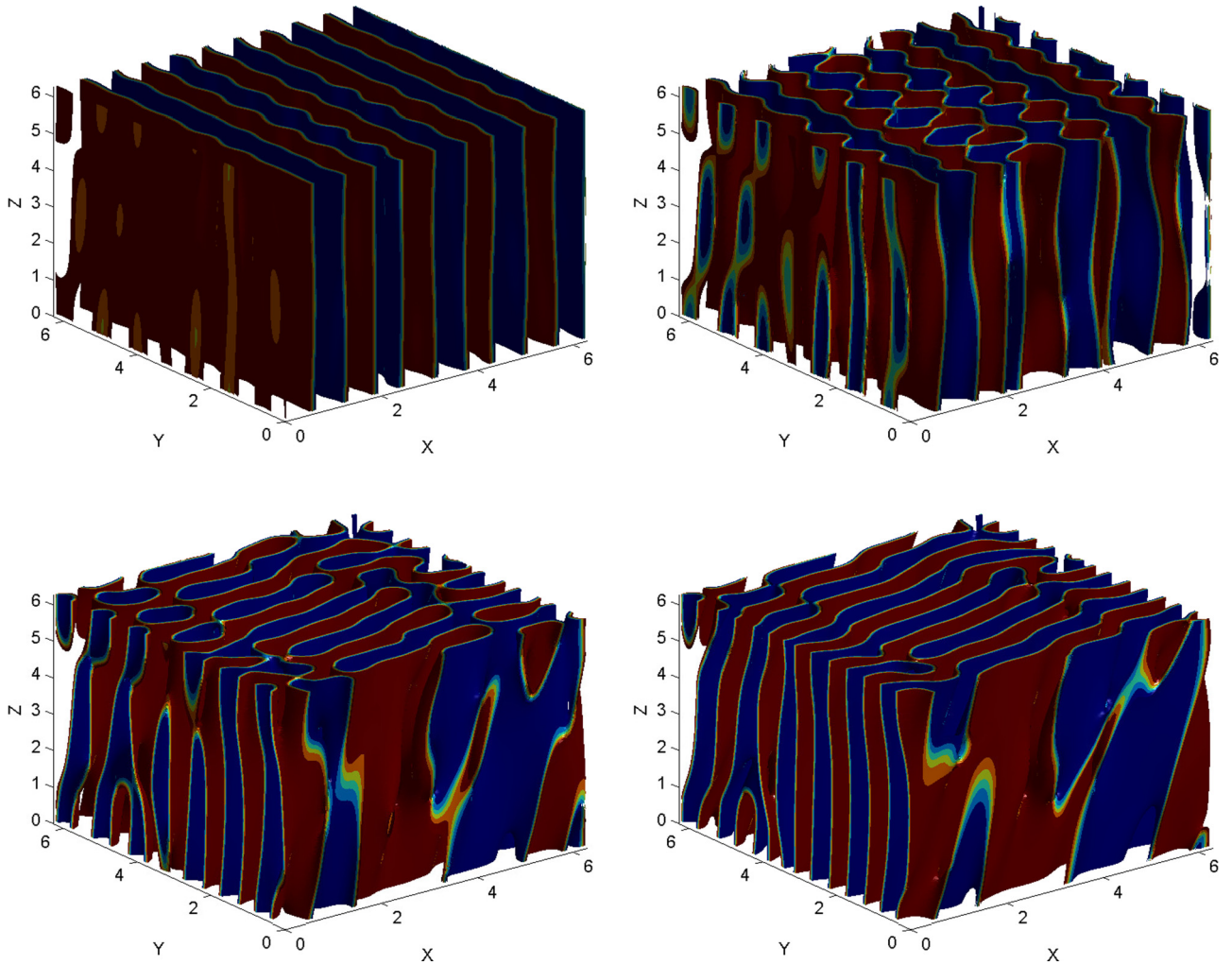

FIG. 7. Three-dimensional solution same as Fig. 6 but here the orientation of the electric field is at 20 degrees with respect to the initial lamellar orientation. The nonlinear evolution is captured for the different times $t = 32,40,48,56$ from left to right and top to bottom.

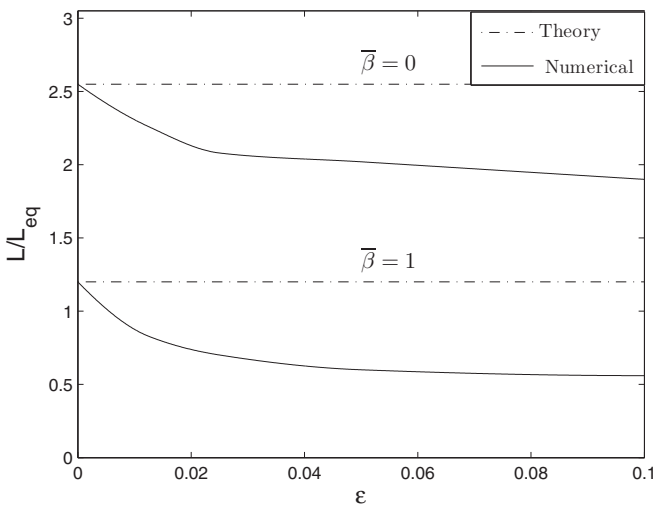

FIG. 8. Effects of finite ϵ on the instability of lamellar patterns. The top and bottom dashed lines correspond to the analytical sharp-interface prediction, and solid lines represent the numerically determined threshold values for various ϵ.

result of Tsori and Andelman [39] for the sharp interface regime. On the other hand, they predict that the varicose mode should dominate in the case of weak segregation, in contradiction to the earlier calculation of Onuki and Fukuda [19].

Over short times, interface alignment appears to occur only in the direction of the imposed field. It was demonstrated that this does not necessarily lead to well-ordered structures in three dimensions. Various strategies for directed assembly, such as alternating the field direction, might be successful in accomplishing complete reorientation of lamellar structures.

There are various extensions of this work which could address other phenomenon related to electric field alignment. For example, the alignment of lamellar microstructures with electric fields may be enhanced in the presence of mobile ions [17,40], or by addition of nanoparticles [41]. Morphological transitions, such as those between spherical, cylindrical and gyroid BCP phases, may also be initiated by applying external fields [7,28]. These transitions are associated with field-induced anisotropic distortions, which stretch and reconfigure pattern domains, rather than instabilities. Our methodology could provide information about stability and bifurcation of these stretched phases.

ACKNOWLEDGMENTS

S.O. was supported through a NSF-Alliance Postdoctoral award DMS-0946431. K.G. was supported through NSF award DMS-1514689.

APPENDIX A

Here we provide details about the expansion of the electrostatic energy term for situations where permittivity weakly depends on composition. We consider this limit both for the diffuse interface free energy (2) as well as the sharp interface case. We show, in particular, that these limits commute, which is to say that the weak composition approximation is valid for the free boundary problem as well.

Weak compositional dependence is introduced by setting setting $\varepsilon(\psi) = \varepsilon_0(\delta\psi)$ where $\delta \ll 1$, and expanding as

$$V = E\mathbf{a}\cdot x + \delta V_1 + \delta V_2 + \cdots$$
$$\varepsilon(\psi) = \varepsilon_0(0) + \delta\varepsilon_0'(0)\psi + \delta^2\varepsilon_0''(0)\psi^2 + \cdots .$$

It is then straightforward to compute

$$\Delta V_1 = -\frac{E\varepsilon_0'(0)}{\varepsilon_0(0)}\nabla\psi\cdot\mathbf{a}, \tag{A1}$$

which is the same as (1). The first two orders of the electrostatic energy expansion are

$$-\frac{1}{2}\int_\Omega E^2\,d\mathbf{x} - \frac{\delta}{2}\int_\Omega \varepsilon_0'(0)E^2\psi + \varepsilon_0(0)E\mathbf{a}\cdot\nabla V_1\,d\mathbf{x},$$

which after integration are simply constants. The $O(\delta^2)$ term in the electrostatic energy is

$$-\frac{1}{2}\int_\Omega \varepsilon_0(0)|\nabla V_1|^2 + 2E\varepsilon_0'(0)\psi\nabla V_1\cdot\mathbf{a} + \varepsilon_0''(0)\psi^2E^2\,d\mathbf{x}. \tag{A2}$$

Note that by using (A1),

$$\int_\Omega \psi\nabla V_1\cdot\mathbf{a}d\mathbf{x} = -\int_\Omega V_1\nabla\psi\cdot\mathbf{a}\,d\mathbf{x} = \frac{\varepsilon_0(0)}{\varepsilon_0'(0)E}\int_\Omega V_1\Delta V_1\,d\mathbf{x}$$
$$= -\frac{\varepsilon_0(0)}{\varepsilon_0'(0)E}\int_\Omega |\nabla V_1|^2\,d\mathbf{x}.$$

Therefore the total contribution of the first two terms of (A2) is $+\varepsilon_0(0)/2\int_\Omega|\nabla V_1|^2\,d\mathbf{x}$, which gives (2).

The last term in (A2) is a a bulk energy contribution proportional to ψ^2. Typically, $\varepsilon(\psi)$ is taken to be a linear function of composition [17,20], in which case this term can be ignored. On the other hand, for nonpolar media theoretical arguments can be made that $\varepsilon'' > 0$, which means that applied field would yield lower energy in the presence of composition fluctuations [7]. Curiously, the opposite effect, mixing of polymer constituents, is often observed instead; this is attributed to the tensorial character of the true relationship between electric and displacement fields [7]. This term is suppressed in our model, although if it were included, it would simply modify the bulk potential and produce a quantifiable change in the sharp interface interphase surface energy.

Finally, we show that the same approximation can be applied in the situation of sharp interfaces. Letting $V = E\mathbf{a}\cdot\mathbf{x} + V_p$ be the original (unscaled) potential, the exact electrostatic energy is

$$-\frac{1}{2}\int_\Omega \varepsilon_\pm(E^2 + 2E\nabla V_p\cdot\mathbf{a} + |\nabla V_p|^2)\,d\mathbf{x}, \tag{A3}$$

where $\varepsilon_\pm$ equals $\varepsilon(\psi = 1)$ on subdomain Ω_+ and equals $\varepsilon_- = \varepsilon(\psi = 0) = \varepsilon_0(0)$ on subdomain Ω_-. The periodic part of the potential solves $\Delta V_p = 0$ on subdomains $\Omega_\pm$ with boundary conditions

$$[\varepsilon_\pm\nabla V_p\cdot\mathbf{n}]_-^+ = -E(\varepsilon_+ - \varepsilon_-)(\mathbf{a}\cdot\mathbf{n}). \tag{A4}$$

The second term in (A3) can be computed by observing

$$\int_\Omega \varepsilon_\pm\nabla V_p\cdot\mathbf{a}\,d\mathbf{x} = \int_\Gamma V_p[\varepsilon_- - \varepsilon_+](\mathbf{a}\cdot\mathbf{n})\,d\mathbf{x}$$
$$= \int_\Gamma V_p[\varepsilon_\pm\nabla V_p\cdot\mathbf{n}]_-^+\,d\mathbf{x}$$
$$= -\int_\Omega \epsilon_\pm|\nabla V_p|^2 d\mathbf{x},$$

where the divergence theorem and condition (A4) was used. Therefore the nonconstant part of the electrostatic energy is exactly

$$\frac{1}{2}\int_\Omega \varepsilon_\pm|\nabla V_p|^2\,d\mathbf{x}. \tag{A5}$$

With $\delta = \varepsilon_+ - \varepsilon_-$, writing $V_p = \delta V_1 + O(\delta^2)$ means that $\Delta V_1 = 0$ on subdomains $\Omega_\pm$ with boundary condition

$$\epsilon_0(0)[\nabla V_1\cdot\mathbf{n}]_-^+ = -E(\mathbf{a}\cdot\mathbf{n}).$$

Thus $\Delta V_1 = E(\mathbf{a}\cdot\mathbf{n})\delta_\Gamma$, which is just the rescaled version of (16). Moreover, at leading order the electrostatic energy (A5) is simply $(\epsilon_0(0)/2)\int_\Omega|\nabla V_1|^2\,d\mathbf{x}$. Therefore the weak compositional dependence approximation also applies when interfaces are sharp.

APPENDIX B

Here we provide details of the sharp interface derivation of Sec. III.

1. Outer solution

The leading order equations are

$$O(\epsilon^0): \begin{cases}\Delta v_0 = 0\\ v_0 = -2u_0\left(1 - u_0^2 big\right)\end{cases}.$$

Matching with the inner solution gives $u_0 = \pm 1$ and $v_0 = 0$. At next order one has

$$O(\epsilon^1): \begin{cases}\Delta v_1 + \alpha(\bar{u} - u_0) + \beta(\nabla^2 u_0\cdot\mathbf{a})\cdot\mathbf{a} = 0\\ v_1 = -2u_1\left(1 - 3u_0^2\right)\end{cases}.$$

Using the outer solution at first order, this above reduces to

$$O(\epsilon^1): \begin{cases}\Delta v_1 = -\alpha(\bar{u} - u_0)\\ v_1 = 4u_1\end{cases}.$$

2. Inner solution

The relationship between inner and outer expansions is given by standard matching conditions for $\rho \to \pm\infty$,

$$\begin{aligned} U_0(\pm\infty,s,t) =& u_0(0\pm,s,t),\\ U_1(\rho,s,t) \sim& u_1(0\pm,\cdot) + \rho u_{0r}(0\pm,\cdot),\\ U_2(\rho,\cdot) \sim& u_2(0\pm,\cdot) + \rho u_{1r}(0\pm,\cdot) + \rho^2/2 u_{0rr}(0\pm,\cdot) \end{aligned}$$

with similar conditions for other quantities. The governing equations in stretched, fitted coordinates read

$$\begin{aligned} &\epsilon^2 r_t U_\rho + \epsilon^3 U_t + \epsilon^3 s_{1t} U_{s_1} + \epsilon^3 s_{2t} U_{s_2}\\ &\quad = V_{\rho\rho} + \epsilon\Delta r V_\rho + \epsilon^2 \Delta s_1 V_{s1} + \epsilon^2 \Delta s_2 V_{s2} + \epsilon^2 V_{s1s1}|\nabla s_1|^2 + \epsilon^2 V_{s2s2}|\nabla s_2|^2 + \epsilon^3\alpha(\bar{U} - U)\\ &\qquad + \epsilon\beta[u_{\rho\rho}(\nabla r\cdot\mathbf{a})^2 + \epsilon^2 u_{s1s1}(\nabla s_1\cdot\mathbf{a})^2 + \epsilon^2 u_{s2s2}(\nabla s_2\cdot\mathbf{a})^2 + 2\epsilon u_{\rho s1}(\nabla r\cdot\mathbf{a})(\nabla s_1\cdot\mathbf{a}) + 2\epsilon u_{\rho s2}(\nabla r\cdot\mathbf{a})(\nabla s_2\cdot\mathbf{a})\\ &\qquad + \epsilon u_\rho(\nabla^2 r\cdot\mathbf{a})\cdot\mathbf{a} + \epsilon^2 u_{s1}(\nabla^2 s_1\cdot\mathbf{a})\cdot\mathbf{a} + \epsilon^2 u_{s2}(\nabla^2 s_2\cdot\mathbf{a})\cdot\mathbf{a}],\\ V =& -U_{\rho\rho} - \epsilon\Delta r U_\rho - \epsilon^2|\nabla s_1|^2 U_{s1s1} - \epsilon^2|\nabla s_2|^2 U_{s2s2} - \epsilon^2\Delta s_1 U_{s1} - \epsilon^2\Delta s_2 U_{s2} - 2U(1-U^2). \end{aligned}$$

Standard formulas from differential geometry give

$$\begin{aligned} \Delta r &= \kappa + O(r),\\ (\nabla^2 r\cdot\mathbf{a})\cdot\mathbf{a} &= \kappa_1(\mathbf{a}\cdot\mathbf{t}_1)^2 + \kappa_2(\mathbf{a}\cdot\mathbf{t}_2)^2 + O(r). \end{aligned}$$

The leading order inner problem and matching conditions are

$$O(\epsilon^0): \begin{cases} V_{0\rho\rho} = 0\\ V_0 = -U_{0\rho\rho} - 2U_0 + 2U_0^3\\ U_0(\pm\infty,\cdot) = u_0(0\pm,\cdot) = \pm 1\\ V_0(\pm\infty,\cdot) = v_0(0\pm,\cdot) = 0 \end{cases}.$$

By the standard common tangent construction [34], $V_0 = 0$ and the second equation is an integrable equation with solution $U_0(\rho,\cdot) = \tanh(\rho)$. At next order,

$$O(\epsilon^1): \begin{cases} V_{1\rho\rho} + \beta(\mathbf{n}\cdot\mathbf{a})^2 U_{0\rho\rho} = 0,\\ \mathcal{L}U_1 = \kappa U_{0\rho} + V_1,\\ \mathcal{L}U_1 \equiv -U_{1\rho\rho} - 2U_1(1-3U_0^2),\\ U_1(\rho,\cdot) \sim u_1(0\pm,\cdot) + \rho u_{0r}(0\pm,\cdot),\ \rho\to\pm\infty\\ V_1(\rho,\cdot) \sim v_1(0\pm,\cdot) + \rho v_{0r}(0\pm,\cdot),\ \rho\to\pm\infty. \end{cases}$$

Integration of the first equation gives $V_1 = \beta(\mathbf{n}\cdot\mathbf{a})^2(-U_0 \pm 1) + v_1(0\pm,\cdot)$, and a solvability condition for the second equation gives

$$\begin{aligned} \langle f, U_{0\rho}\rangle &= \langle \mathcal{L}U_1, U_{0\rho}\rangle = \langle -V_1 - \kappa U_{0\rho}, U_{0\rho}\rangle\\ &= \int_{-\infty}^{\infty} (-V_1 U_{0\rho} - \kappa U_{0\rho}^2)\, d\rho = 0. \end{aligned}$$

Combining these results gives the boundary condition for v_1 on each side of the interface

$$v_1(0\pm,\cdot) + \beta(\mathbf{n}\cdot\mathbf{a})^2(\pm 1) = -\frac{2}{3}\kappa.$$

Finally, at the next order

$$O(\epsilon^2): \begin{cases} r_{ot} U_{0\rho} = V_{2\rho\rho} + \kappa V_{1\rho} + \beta\left\{U_{1\rho\rho}(\mathbf{n}\cdot\mathbf{a})^2 + 2U_{0\rho\rho}\nabla r\cdot\mathbf{a} U_0\left[\kappa_1(\mathbf{t}_1\cdot\mathbf{a})^2 + \kappa_2(\mathbf{t}_2\cdot\mathbf{a})^2\right]\right\}\\ V_2 = -U_{2\rho\rho} - \kappa U_{1\rho} + 6U_0U_2 + 6U_0U_1^2 - 2U_2\\ U_2(\rho,\cdot) = u_2(0\pm,\cdot) + \rho u_{1r}(0\pm,\cdot)\} + \rho^2/2 u_{0rr}(0\pm,\cdot), \quad \rho\to\pm\infty,\\ V_2(\rho,\cdot) = v_2(0\pm,\cdot) + \rho v_{1r}(0\pm,\cdot)\} + \rho^2/2 v_{0rr}(0\pm,\cdot), \quad \rho\to\pm\infty. \end{cases}$$

The first equation reduces to

$$r_{ot} U_{0\rho} = V_{2\rho\rho} + \beta\{-\kappa(\mathbf{n}\cdot\mathbf{a})^2 U_{0\rho} + U_{1\rho\rho}(\mathbf{n}\cdot\mathbf{a})^2 + 2U_{0\rho\rho}\nabla r\cdot\mathbf{a} + U_{0\rho}[\kappa_1(\mathbf{t}_1\cdot\mathbf{a})^2 + \kappa_2(\mathbf{t}_2\cdot\mathbf{a})^2]\}.$$

Integrating in ρ and matching leads to Eq. (8).

APPENDIX C

Details of the energy dissipation expression (17) are given. First, we note two facts about the potentials w and Φ. First, w is continuously differentiable throughout the entire domain. Second, Φ is continuous, but it has a jump discontinuity in its normal derivative

$$[\nabla\Phi\cdot\mathbf{n}]^+_- = 2(\mathbf{n}\cdot\mathbf{a}) \tag{C1}$$

so that

$$[\nabla\Phi\cdot\mathbf{a}]^+_- = (\mathbf{n}\cdot\mathbf{a})[\nabla\Phi\cdot\mathbf{n}]^+_- = 2(\mathbf{n}\cdot\mathbf{a})^2. \tag{C2}$$

The rate of energy dissipation can be written in terms of the normal front velocity as

$$\frac{dE}{dt} = \int_\Gamma \left[\frac{4}{3}\kappa - 2\alpha w - \beta(\nabla\Phi\cdot\mathbf{a})^+_-\right] V_n(s)\,ds,$$

where $()^+_-$ denotes the sum of a quantity on either side of the interface. Using the boundary condition (11) and (C2),

$$\frac{dE}{dt} = \int_\Gamma -2\left[v \pm \frac{1}{2}\beta[\nabla\Phi\cdot\mathbf{a}]^+_- + \alpha w + \frac{1}{2}\beta(\nabla\Phi\cdot\mathbf{a})^+_-\right] \times V_n(s)\,ds, \tag{C3}$$

where $+$ is used if v is evaluated from the Ω_+ side of the interface, and minus for Ω_-. It follows that the term in brackets can be identified as the limit of the total chemical potential

$$\mu = v + \alpha w + \mu_e, \quad \mu_e \equiv \beta\nabla\Phi\cdot\mathbf{a}$$

as Γ is approached from either side. Using (15) and (16), note that $\Delta\mu = 0$ on either subdomain $\Omega_\pm$.

The interface velocity arises from a jump in the normal derivative of the chemical potential across the interface as $V_n = -\frac{1}{2}[\partial\mu/\partial n]^+_-$. We can show how the second term in the velocity expression (12) arises from gradients of μ_e. Using the boundary fitted coordinates (r,s_1,s_2) it follows

$$[\partial\mu_e/\partial n]^+_- = \beta[(\nabla^2\cdot\mathbf{a})\cdot\mathbf{n}]^+_- = \beta[\Phi_{rr}(\mathbf{n}\cdot\mathbf{a}) + \Phi_{rs_1}(\mathbf{t}_1\cdot\mathbf{a}) + \Phi_{rs_2}(\mathbf{t}_2\cdot\mathbf{a})]^+_-. \tag{C4}$$

Then using formula (C1),

$$[\Phi_{rs_j}(\mathbf{a}\cdot\mathbf{t}_j)]^+_- = \frac{\partial}{\partial s_j}[\Phi_r(\mathbf{a}\cdot\mathbf{t}_j)]^+_- = 2\frac{\partial}{\partial s_j}(\mathbf{n}\cdot\mathbf{a}) = 2\kappa_j(\mathbf{t}_j\cdot\mathbf{a}). \tag{C5}$$

Away from the interface, $\Delta\Phi = 0$, which in fitted coordinates reads

$$\Phi_{rr} + (\Delta r)\Phi_r + (\Delta s_1)\Phi_{s1} + |\nabla s_1|^2\Phi_{s1s1} + (\Delta s_2)\Phi_{s2} + |\nabla s_2|^2\Phi_{s2s2} = 0. \tag{C6}$$

Since Φ_{s_j} and $\Phi_{s_js_j}$ are continuous across the interface and Δr limits to κ on the interface, it follows that

$$[\Phi_{rr}]^+_- = -\kappa[\Phi_r]^+_- = -2\kappa(\mathbf{n}\cdot\mathbf{a}). \tag{C7}$$

Combining (C4), (C5), and (C7)

$$[\partial\mu_e/\partial n]^+_- = -2\beta\kappa(\mathbf{n}\cdot\mathbf{a}) + 2\beta[\kappa_1(\mathbf{t}_1\cdot\mathbf{a}) + \kappa_2(\mathbf{t}_2\cdot\mathbf{a})], \tag{C8}$$

which leads to the electric field contribution in (12). Finally, returning to the energy dissipation expression (C3), it can be written using the Green's identity (with the same sign convention for the normal to the boundary) as (17).

[1] T. Smart, H. Lomas, M. Massignani, M. V. Flores-Merino, L. Ruiz Perez, and G. Battaglia, Block copolymer nanostructures, Nano Today **3**, 38 (2008).

[2] H.-C. Kim, S.-M. Park, and W. D. Hinsberg, Block copolymer based nanostructures: materials, processes, and applications to electronics, Chem. Rev. **110**, 146 (2010).

[3] J. K. Kim, S. Y. Yang, Y. Lee, and Y. Kim, Functional nanomaterials based on block copolymer self-assembly, Prog. Polymer Sci. **35**, 1325 (2010).

[4] S. B. Darling, Directing the self-assembly of block copolymers, Prog. Polymer Sci. **32**, 1152 (2007).

[5] M. P. Stoykovich, M. Müller, S. O. Kim, H. H. Solak, E. W. Edwards, J. J. De Pablo, and P. F. Nealey, Directed assembly of block copolymer blends into nonregular device-oriented structures, Science **308**, 1442 (2005).

[6] S. Sakurai, Progress in control of microdomain orientation in block copolymers–efficiencies of various external fields, Polymer **49**, 2781 (2008).

[7] C. Liedel, C. W. Pester, M. Ruppel, V. S. Urban, and A. Böker, Beyond orientation: The impact of electric fields on block copolymers, Macromol. Chem. Phys. **213**, 259 (2012).

[8] Y. Tsori, Colloquium: Phase transitions in polymers and liquids in electric fields, Rev. Modern Phys. **81**, 1471 (2009).

[9] K. Amundson, E. Helfand, X. Quan, S. D. Hudson, and S. D. Smith, Alignment of lamellar block copolymer microstructure in an electric field. 2. Mechanisms of alignment, Macromolecules **27**, 6559 (1994).

[10] A. V. Kyrylyuk, A. V. Zvelindovsky, G. J. A. Sevink, and J. G. E. M. Fraaije, Lamellar alignment of diblock copolymers in an electric field, Macromolecules **35**, 1473 (2002).

[11] T. Thurn-Albrecht, J. DeRouchey, T. P. Russell, and R. Kolb, Pathways toward electric field induced alignment of block copolymers, Macromolecules **35**, 8106 (2002).

[12] K. Schmidt, A. Böker, H. Zettl, F. Schubert, H. Hänsel, F. Fischer, T. M. Weiss, V. Abetz, A. V. Zvelindovsky, G. J. A. Sevink *et al.*, Influence of initial order on the microscopic mechanism of electric field induced alignment of block copolymer microdomains, Langmuir **21**, 11974 (2005).

[13] C.-Y. Lin and M. Schick, Self-consistent field study of the alignment by an electric field of a cylindrical phase of block copolymer, J. Chem. Phys. **125**, 034902 (2006).

[14] C.-Y. Lin, M. Schick, and D. Andelman, Structural changes of diblock copolymer melts due to an external electric field: A self-consistent-field theory study, Macromolecules **38**, 5766 (2005).

[15] K. Schmidt, H. G. Schoberth, M. Ruppel, H. Zettl, H. Hänsel, T. M. Weiss, V. Urban, G. Krausch, and A. Böker, Reversible

tuning of a block-copolymer nanostructure via electric fields, Nat. Mater. **7**, 142 (2007).
[16] K. S. Lyakhova, A. V. Zvelindovsky, and G. J. A. Sevink, Kinetic pathways of order-to-order phase transitions in block copolymer films under an electric field, Macromolecules **39**, 3024 (2006).
[17] Y. Tsori, F. Tournilhac, and L. Leibler, Orienting ion-containing block copolymers using ac electric fields, Macromolecules **36**, 5873 (2003).
[18] M. W. Matsen, Electric field alignment in thin films of cylinder-forming diblock copolymer, Macromolecules **39**, 5512 (2006).
[19] A. Onuki and J.-I. Fukuda, Electric field effects and form birefringence in diblock copolymers, Macromolecules **28**, 8788 (1995).
[20] M. W. Matsen, Stability of a Block-Copolymer Lamella in a Strong Electric Field, Phys. Rev. Lett. **95**, 258302 (2005).
[21] M. W. Matsen, Undulation instability in block-copolymer lamellae subjected to a perpendicular electric field, Soft Matter **2**, 1048 (2006).
[22] T. Ohta and K. Kawasaki, Equilibrium morphology of block coploymer melts, Macromolecules **19**, 2621 (1986).
[23] R. Choksi, M. A. Peletier, and J. F. Williams, On the phase diagram for microphase separation of diblock copolymers: An approach via a nonlocal Cahn-Hilliard functional, SIAM J. Appl. Math. **69**, 1712 (2009).
[24] Y. Nishiura and I. Ohnishi, Some mathematical aspects of the micro-phase separation of diblock copolymers, Physica D **84**, 31 (1995).
[25] C. B. Muratov, Theory of domain patterns in systems with long-range interactions of Coulomb type, Phys. Rev. E **66**, 066108 (2002).
[26] T. Xu, A. V. Zvelindovsky, G. J. A. Sevink, O. Gang, B. Ocko, Y. Zhu, S. P. Gido, and T. P. Russell, Electric field induced sphere-to-cylinder transition in diblock copolymer thin films, Macromolecules **37**, 6980 (2004).
[27] A. V. Kyrylyuk, G. J. A. Sevink, A. V. Zvelindovsky, and J. G. E. M. Fraaije, Simulations of electric field induced lamellar alignment in block copolymers in the presence of selective electrodes, Macromol. Theory Simulations **12**, 508 (2003).
[28] M. Pinna and A. V. Zvelindovsky, Kinetic pathways of gyroid-to-cylinder transitions in diblock copolymers under external fields: Cell dynamics simulation, Soft Matter **4**, 316 (2008).
[29] M. Pinna, A. V. Zvelindovsky, S. Todd, and G. Goldbeck-Wood, Cubic phases of block copolymers under shear and electric fields by cell dynamics simulation. I. Spherical phase, J. Chem. Phys. **125**, 154905 (2006).
[30] X.-F. Wu and Y. A. Dzenis, Phase-field modeling of the formation of lamellar nanostructures in diblock copolymer thin films under inplanar electric fields, Phys. Rev.E **77**, 031807 (2008).
[31] X. Ren and J. Wei, On the spectra of three-dimensional lamellar solutions of the diblock copolymer problem, SIAM J. Math. Anal. **35**, 1 (2003).
[32] R. Choksi and X. Ren, On the derivation of a density functional theory for microphase separation of diblock copolymers, J. Statist. Phys. **113**, 151 (2003).
[33] K. Amundson, E. Helfand, X. Quan, and S. D. Smith, Alignment of lamellar block copolymer microstructure in an electric field. 1. Alignment kinetics, Macromolecules **26**, 2698 (1993).
[34] R. L. Pego, Front migration in the nonlinear Cahn-Hilliard equation, Proc. R. Soc. Lond. A **422**, 261 (1989).
[35] A. N. Semenov, Microphase separation in diblock copolymer melts: Ordering of micelles, Macromolecules **22**, 2849 (1989).
[36] G. M. Grason, The packing of soft materials: Molecular asymmetry, geometric frustration and optimal lattices in block copolymer melts, Phys. Rep. **433**, 1 (2006).
[37] K. Glasner and S. Orizaga, Improving the accuracy of convexity splitting methods for gradient flow equations, J. Comput. Phys. **315**, 52 (2016).
[38] M. Pinna, L. Schreier, and A. V. Zvelindovsky, Mechanisms of electric-field-induced alignment of block copolymer lamellae, Soft Matter **5**, 970 (2009).
[39] Y. Tsori and D. Andelman, Thin film diblock copolymers in electric field: Transition from perpendicular to parallel lamellae, Macromolecules **35**, 5161 (2002).
[40] A. Dehghan, M. Schick, and A.-C. Shi, Effect of mobile ions on the electric field needed to orient charged diblock copolymer thin films, J. Chem. Phys. **143**, 134902 (2015).
[41] L.-T. Yan, H. G. Schoberth, and A. Böker, Lamellar microstructure and dynamic behavior of diblock copolymer/nanoparticle composites under electric fields, Soft Matter **6**, 5956 (2010).